Dilute nitride based double-barrier quantum wells for intersubband absorption at 1.31 and 1.55 μm

Y. X. Dang and W. J. Fan*

School of Electrical and Electronic Engineering, Nanyang Technological University, Singapore 639798, Singapore

(Received 3 May 2007; revised manuscript received 19 September 2007; published 25 March 2008)

A systematic investigation of intersubband optical absorptions in $In_xGa_{1-x}As_{1-y}N_y/AlAs/Al_zGa_{1-z}As$ double-barrier quantum well (DBQW) structures is reported. Electron subbands and the energy dependent effective potential for the envelope wave functions are calculated by means of the ten-band $k\cdot p$ scheme, which takes into account the effects of subband nonparabolicity and strain. From the calculations of the energy dispersions and wave functions of the respective states, we find that when the conduction-band offset is very large such that the first excited state lies above the localized nitrogen level, each of the ground and the first excited states is split into two levels. The intersubband absorptions in the DBQW structure have been studied by varying the well width and the compositions of the alloys. The strongest calculated absorption peak corresponding to the transition from the ground level to the higher excited level shows the same peculiarities. Finally, DBQW structures, which correspond to 1.31 and 1.55 μm intersubband absorptions, respectively, have been achieved.

DOI: 10.1103/PhysRevB.77.125334 PACS number(s): 73.21.Fg, 73.63.Hs, 78.67.De

I. INTRODUCTION

Over the past few years, a considerable number of studies have been done on GaAs-based quantum well infrared photodetectors (QWIPs). One of the main advantages of QWIPs is the possibility of working in the 3–5 and 8–12 μm atmospheric transmission wave bands by changing their structures, which are well documented in Ref. 1. In view of optical fiber communications, QWIPs designed for operating in the 1.31–1.55 μm region are highly expected. Due to their inherently short carrier lifetime, the intersubband transition (ISBT)-based QWIPs may offer a higher speed capability than the standard approach based on interband transitions. Although there have been some observations of the intersubband transition in such a short wavelength region,[2] a systematic theoretical study is still lacking.

The present paper reports our attempts to achieve the 1.31–1.55 μm intersubband transitions by using a dilute nitride based material system grown on GaAs substrates. There are two routes to achieving the desired wavelengths based on GaAs substrates: One route is to seek a conduction-band offset (CBO) as large as one can obtain, and the other route is to change the excited state into a resonant state confined by thin tunneling barriers. The first solution, which is extensively applied and is known as a single quantum well (SQW) structure, uses the $In_xGa_{1-x}As/Al_zGa_{1-z}As$ system in the early stage. The shortest wavelength that can be achieved by using this scheme is around 1.26 μm.[3] The second approach utilizes a double-barrier quantum well (DBQW) structure.[4–12] Instead of a single layer as the barrier, this structure uses two thin layers with an extremely large band gap and is further separated by a layer with a smaller band gap to form a combined barrier. Devices based on such a design exhibit low dark current and a photovoltaic behavior due to the existence of unintentional asymmetries and an internal electric field as compared to the SQW devices.[13] Luna *et al.*[14] demonstrated QWIPs operating at a wavelength as short as 1.64 μm by applying this DBQW structure with the $GaAs_{1-x}N_x/AlAs/Al_zGa_{1-z}As$ system.

Here, we further explore using a similar DBQW structure for 1.31–1.55 μm operation. The material system investigated is the $In_xGa_{1-x}As_{1-y}N_y/AlAs/Al_zGa_{1-z}As$ heterostructure. The superior properties of this system relative to the extensively used N-free system can be accounted for by the fact that adding a small amount of nitrogen atoms into the InGaAs matrix to form $In_xGa_{1-x}As_{1-y}N_y$ is found to greatly reduce the band gap energy and simultaneously reduce the compressive strain present in the well layer.[15] Additionally, the incorporation of N exclusively affects the CBO, leaving the valence-band offset unchanged. With the same concentration of indium, the CBO of the heterostructure increases by more than 200 meV with only 2% N content being introduced.[16] Therefore, this intriguing aspect of nitrogen leads to the possibility of achieving 1.31–1.55 μm absorption by using the $In_xGa_{1-x}As_{1-y}N_y/Al_zGa_{1-z}As$ system due to its large CBO of up to 1.5 eV.

II. THEORETICAL APPROACH

A. Double-barrier quantum well band structure calculation

The eigenstates of the DBQW structures satisfy the Schrödinger equation,

$$H\Psi = E\Psi, \tag{1}$$

where Ψ is the total wave function. Within the framework of the ten-band $k\cdot p$ model, the ten-dimensional electron and hole envelope wave functions for the quantum wells (QWs) are written as

$$\Phi_n = \{\Phi_n^j\}, \quad (j = 1,2,\ldots,10), \tag{2}$$

where the components of Φ_n^j are given by

$$\Phi_n^j = \exp[i(k_x x + k_y y)] \sum_m a_{n,m}^j \frac{1}{\sqrt{L}} \exp\left[i\left(k_z + m\frac{2\pi}{L} \right) z \right], \tag{3}$$

where $L=\mathrm{ww}+2\mathrm{bw1}+\mathrm{bw2}$ designates the periodicity of the DBQW. We use ww to indicate the width of the central quantum well and bw1 and bw2 to represent the widths of the inner and outer barrier layers, respectively. k_x, k_y, and k_z are the wave vectors, n is the index for the respective energy levels, $a_{n,m}^j$ is the expansion coefficient, and z is the coordinate in the growth direction. The total wave function Ψ is the product of the envelope wave functions in Eq. (2) and the periodic part of the Bloch basis functions at the zone center u_j, as listed below:

$$u_1 = |S_\mathrm{N}\uparrow\rangle, \tag{4a}$$

$$u_2 = |S_\mathrm{N}\downarrow\rangle, \tag{4b}$$

$$u_3 = |S\uparrow\rangle, \tag{4c}$$

$$u_4 = |S\downarrow\rangle, \tag{4d}$$

$$u_5 = -\frac{i}{\sqrt{2}}|(X+iY)\uparrow\rangle, \tag{4e}$$

$$u_6 = -\frac{i}{\sqrt{6}}|[(X+iY)\downarrow - 2Z\uparrow]\rangle, \tag{4f}$$

$$u_7 = \frac{i}{\sqrt{6}}|[(X-iY)\uparrow + 2Z\downarrow]\rangle, \tag{4g}$$

$$u_8 = \frac{i}{\sqrt{2}}|(X-iY)\downarrow\rangle, \tag{4h}$$

$$u_9 = \frac{i}{\sqrt{3}}|[(X+iY)\downarrow + Z\uparrow]\rangle, \tag{4i}$$

$$u_{10} = \frac{i}{\sqrt{3}}|[(X-iY)\uparrow - Z\downarrow]\rangle, \tag{4j}$$

where $|X\rangle$, $|Y\rangle$, $|Z\rangle$, and $|S\rangle$ are the orbital wave functions of the top of the valence band and the bottom of the conduction band, respectively. $\uparrow$ and $\downarrow$ denote the spin-up and spin-down components, respectively.

In order to identify the nitrogen (N), electron (e), heavy hole (HH), light hole (LH), and spin-orbit (SO) split-off band components in the energy states of the DBQW, we introduce the following probability functions:

$$P_n^\mathrm{N} = \sum_{j=1,2} \sum_m a_{n,m}^{j*} a_{n,m}^j, \tag{5a}$$

$$P_n^e = \sum_{j=3,4} \sum_m a_{n,m}^{j*} a_{n,m}^j, \tag{5b}$$

$$P_n^\mathrm{HH} = \sum_{j=5,8} \sum_m a_{n,m}^{j*} a_{n,m}^j, \tag{5c}$$

$$P_n^\mathrm{LH} = \sum_{j=6,7} \sum_m a_{n,m}^{j*} a_{n,m}^j, \tag{5d}$$

$$P_n^\mathrm{SO} = \sum_{j=9,10} \sum_m a_{n,m}^{j*} a_{n,m}^j. \tag{5e}$$

By calculating P_n^N, P_n^e, P_n^HH, P_n^LH, and P_n^SO, the components of the nitrogen, electron, heavy hole, light hole, and spin-orbit split-off states in the DBQW can be known. These probability functions are particularly useful in identifying the dominant character in a particular energy state. However, the following sum rule is valid:

$$\sum_i P_n^i = 1, \quad i = \mathrm{N}, e, \mathrm{HH}, \mathrm{LH}, \mathrm{SO}. \tag{6}$$

The wave function can be classified into two categories. Φ_{n_c} and Φ_{n_v} belong to the conduction band and valence band, respectively. They are determined according to the positions of the energy subbands and the calculated probability functions.

B. Mathematical formulation of the optical absorption in double-barrier quantum well systems

The optical intersubband transition rate is proportional to the momentum matrix element,

$$M_{nn'} = \langle \Psi_n | \mathbf{e_v} \cdot \mathbf{P} | \Psi_{n'} \rangle = \sum_{j,j'=1}^{10} [\langle \Phi_{nj} | \mathbf{e_v} \cdot \mathbf{P} | \Phi_{n'j'} \rangle \langle u_j | u_{j'} \rangle + \langle \Phi_{nj} | \Phi_{n'j'} \rangle \langle u_j | \mathbf{e_v} \cdot \mathbf{P} | u_{j'} \rangle], \tag{7}$$

where $\mathbf{e_v} = v_x e_x + v_y e_y + v_z e_z (v_x^2 + v_y^2 + v_z^2 = 1)$ is the unit vector in the direction of the electric field, $\mathbf{P}$ is the momentum operator, Φ is the envelope wave function, and Ψ is the total electron wave function derived from Eq. (1). Subscripts n and n' are the index of the initial state and the final state of the intersubband transitions, respectively. u_j has been defined in Eqs. (4a)–(4j). In Eq. (7), the part before the plus sign represents the transitions occurring within the same Bloch basis states, namely, intraband transitions, while the other part represents the transitions occurring from the coupling of $|S\rangle$ and $|X\rangle$, $|Y\rangle$, and $|Z\rangle$ Bloch basis states, which are known as interband transitions. The optical absorption coefficient $\alpha_{nn'}(\hbar\omega)$ can be obtained from

$$\alpha_{nn'}(\hbar\omega) = \frac{\pi e^2}{n_r c \varepsilon_0 m_0^2 \omega} \frac{2}{V} \sum_{k_t} |M_{nn'}|^2 \delta(E_{n'} - E_n - \hbar\omega)(f_n - f_{n'}), \tag{8}$$

where n_r is the refractive index, c is the light speed, ε_0 is the free-space dielectric constant, m_0 is the free electron mass, ω is the photon frequency, and V is the volume of the integral space. $k_t=(k_x,k_y)$ is a two-dimensional in-plane wave vector. $\delta(E_{n'}-E_n-\hbar\omega)$ may be replaced by a Lorentzian function with a linewidth Γ when the scattering relaxation is taken into account, and it becomes

TABLE I. Parameters for binary compounds used in the calculation.

Parameters	GaAs[a]	AlAs[a]	InAs[a]	GaN[b]	InN[b]
Lattice constant a_0 (Å)	5.6533	5.6611	6.0584	4.5000	4.9800
Spin-orbit splitting energy Δ_0 (eV)	341	280	390	17	5
Optical matrix parameter E_p (eV)	28.8	21.1	21.5	25.0	17.2
Deformation potential constant a_c (eV)	−7.17	−5.64	−5.08	−6.71	−2.65
Deformation potential constant a_v (eV)	1.16	2.47	1.00	0.69	0.70
Shear deformation potential b (eV)	−2.0	−2.3	−1.8	−2.0	−1.2
Elastic constant c_{11} (GPa)	122.10	125.00	83.29	293.00	187.00
Elastic constant c_{12} (GPa)	56.60	53.40	45.26	159.00	125.00
Luttinger parameter γ_1	6.98	3.76	20.00	2.70	3.72
Luttinger parameter γ_2	2.06	0.82	8.50	0.76	1.26
Luttinger parameter γ_3	2.93	1.42	9.20	1.11	1.63
Conduction-band effective mass $m_e^\star$ (m_0)	0.067	0.15	0.026		
Unstrained band gap energy E_g (T=300 K) (eV)	1.422	3.003	0.354		

[a]Reference 20.
[b]Reference 21.

$$\delta(E_{n'} - E_n - \hbar\omega) = \frac{\Gamma}{2\pi\left[(E_{n'} - E_n - \hbar\omega)^2 + \left(\frac{\Gamma}{2}\right)^2\right]}. \quad (9)$$

Finally,

$$f_n = \frac{1}{1 + e^{(E_n - E_F)/k_B T}} \quad (10)$$

is the Fermi–Dirac distribution function for the initial state, where E_n is the subband energy for the initial state and E_F is the quasi-Fermi level. A similar expression holds for the Fermi–Dirac distribution function for the excited state $f_{n'}$, where E_n is replaced by $E_{n'}$.

In order to investigate the absorption coefficients obtainable at a certain carrier density, the corresponding quasi-Fermi levels must be determined from the integration of the density of states in the DBQW. Considering the nonparabolic energy dispersion curves, a determination of carrier density by numerically integrating over the k space is more appropriate, as shown by

$$N = \sum_{n_c} \int \frac{1}{4\pi^2 \mathrm{ww}} f_n[E_n(k_x, k_y)] dk_x dk_y, \quad (11)$$

where N is the electron density. f_n is the Fermi–Dirac distribution for electrons in the conduction band which is given by Eq. (10).

C. Band parameters

The ten-band $k \cdot p$ method was previously applied by us to calculate dilute nitride related alloys, such as InGaAsN (Refs. 15, 17, and 18) and GaAsSbN,[19] and the results show the validity of this model. The description of the ten-band $k \cdot p$ Hamiltonian and the solution of Eq. (1) can be traced throughout our earlier work. Though earlier the model was only applied to the calculations of SQW cases, utilizing it in the calculations of a DBQW structure is straightforward. One only needs to redefine the period L of the DBQW along the growth direction, as mentioned previously. Except for the band gap energies, the electron effective masses, and nitrogen related parameters, most parameters for $In_xGa_{1-x}As_{1-y}N_y$ and $Al_zGa_{1-z}As$ materials are obtained by using a linear interpolation between the parameters of the relevant binary compounds, which can be expressed as

$$P(In_xGa_{1-x}As_{1-y}N_y) = P(GaAs)(1-x)(1-y) + P(InAs)x(1-y) + P(GaN)(1-x)y + P(InN)xy \quad (12)$$

and

$$P(Al_zGa_{1-z}As) = P(GaAs)(1-z) + P(AlAs)z. \quad (13)$$

The parameters used are shown in Table I.[20,21] The band gap energy of $In_xGa_{1-x}As$ is calculated by

$$E_g(In_xGa_{1-x}As) = (1-x)[E_g(GaAs,T)] + x[E_g(InAs,T)] - 0.477(1-x)x, \quad (14)$$

and the band gap energy of $Al_zGa_{1-z}As$ can be calculated from

$$E_g(Al_zGa_{1-z}As) = (1-z)[E_g(GaAs,T)] + z[E_g(AlAs,T)] - (1.31z - 0.127)z(1-z), \quad (15)$$

taking into account the temperature (T) and band gap energies in units of eV. The effective mass m_e^* of $In_xGa_{1-x}As$ is given by

$$m_e^*(In_xGa_{1-x}As) = (1-x)m_e^*(GaAs) + xm_e^*(InAs) - 0.0091x(1-x). \quad (16)$$

TABLE II. Structures for comparison with the literature using the ten-band model and the compared results.

Structure No.	Structure	ww (Å)	bw1 (Å)	bw2 (Å)	bw3 (Å)	T (K)	Expt. (μm)	Calc. (μm)
I	$GaAs_{0.99}N_{0.01}/GaAs/AlAs/Al_{0.3}Ga_{0.7}As$ [a]	30	5	20	300	25	1.64	1.69
II	$GaAs_{0.993}N_{0.007}/GaAs/AlAs/Al_{0.3}Ga_{0.7}As$ [b]	25	5	20	300	300	3	2.94
III	$GaAs_{0.993}N_{0.007}/AlAs/Al_{0.3}Ga_{0.7}As$ [b]	55		20	300	300	2.5	2.46

[a]Reference 14.
[b]Reference 23.

One should note that the bowing factors, 0.477 and 0.0091, in Eqs. (14) and (16), respectively, are recommended by Vurgaftman *et al.*[20] The effective mass m_e^* of $Al_zGa_{1-z}As$ changes with respect to the composition z of Al constituents as

$$m_e^*(Al_zGa_{1-z}As) = 0.083z + 0.067. \quad (17)$$

The band anticrossing model states that the large reduction in the fundamental band gap of $In_xGa_{1-x}As_{1-y}N_y$ is due to the repulsion between a localized nitrogen related energy level (E_N) and the extended conduction band (E_c) of the $In_xGa_{1-x}As$ host matrix. Calculations of the nitrogen related parameters E_N and V_{NC} in units of eV, for $In_xGa_{1-x}As_{1-y}N_y$ material within the ten-band regime, are as follows[21]:

$$E_N = 1.65(1-x) + 1.44x - 0.38x(1-x), \quad (18a)$$

$$V_{NC} = 2.7(1-x) + 2.0x - 3.5x(1-x). \quad (18b)$$

Another important parameter which strongly affects the calculations is the CBO ratio (Q_c). For calculations using the ten-band model, we only need the values of Q_c for $In_xGa_{1-x}As/Al_zGa_{1-z}As$ heterostructures. We select these values from the work of Arent.[22]

III. RESULTS AND DISCUSSIONS

A. Verification of the ten-band $k\cdot p$ method

In order to verify our theoretical model, we have performed some calculations based on the ten-band model and compared them with the reported absorption results in the literature. Up until now, there were only a few studies on $In_xGa_{1-x}As_{1-y}N_y/AlAs/Al_zGa_{1-z}As$ DBQWs. We compared our calculations with the experimental results of Luna *et al.*[14,23] Table II gives out the detailed structures they studied and the results of our comparison. All calculations presented in this paper were done with respect to the valence-band maximum without strain.

Figure 1 illustrates our calculation results on structure I shown in Table II. Luna *et al.* found a responsivity peak located at 1.64 μm under an applied bias of 2 V for this material system. Figure 1(a) shows the squared wave functions. The first four wave functions coming from the GaAsN well are denoted by solid lines. It is interesting to note that two of them have one single peak and the other two have double peaks in the well region, rather than the normal case with a single peak for the ground level, double peaks for the

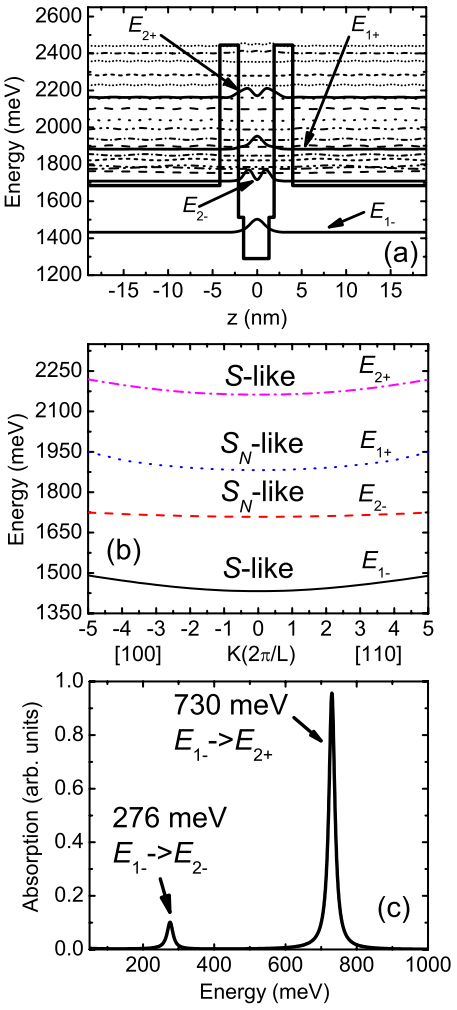

FIG. 1. (Color online) Energy levels and absorption coefficients in a $GaAs_{0.99}N_{0.01}/GaAs/AlAs/Al_{0.3}Ga_{0.7}As$ system with a well width of 30 Å. (a) The squared wave functions correspond to the subbands in the conduction band when $k=0$ ($2\pi/L$). The wave functions confined in the well region (GaAsN) are denoted by solid lines and those confined in the outer barrier region (AlGaAs) are denoted by dashed dotted lines. (b) Dispersions of the subbands in the conduction band of the well (the ground and the first excited levels only). At $k=0$ ($2\pi/L$), the highest and the lowest subbands are identified as S-like, and the other two states are identified as S_N-like. (c) The calculated intersubband transition coefficients as a function of the transition energy at 25 K. The detailed structure is for structure I in Table II.

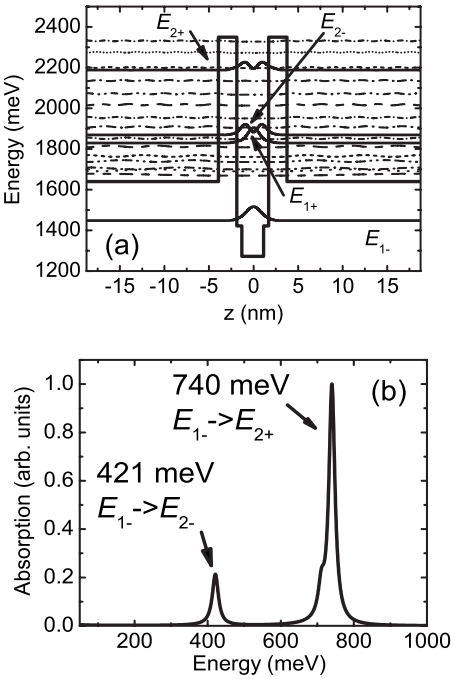

FIG. 2. Energy levels and absorption coefficients in a $GaAs_{0.993}N_{0.007}/GaAs/AlAs/Al_{0.3}Ga_{0.7}As$ system with a well width of 25 Å. (a) The squared wave functions correspond to the subbands in the conduction band when $k=0$ $(2\pi/L)$. The wave functions confined in the well region (GaAsN) are denoted by solid lines and those confined in the outer barrier region (AlGaAs) are denoted by dashed dotted lines. (b) The calculated intersubband absorption coefficients as a function of the transition energy at room temperature. The detailed structure is for structure II in Table II.

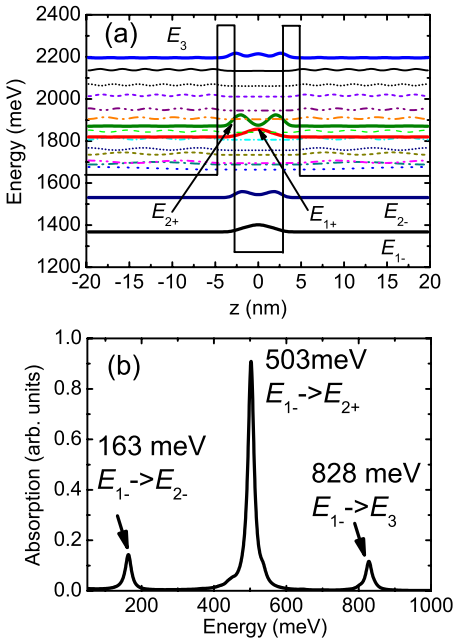

FIG. 3. (Color online) Energy levels and absorption coefficients in a $GaAs_{0.993}N_{0.007}/AlAs/Al_{0.3}Ga_{0.7}As$ DBQW with a well width of 55 Å. (a) The squared wave functions correspond to the subbands in the conduction band when $k=0$ $(2\pi/L)$. The wave functions confined in the well region (GaAsN) are denoted by solid lines and those confined in the outer barrier region (AlGaAs) are denoted by dashed dotted lines. (b) The calculated intersubband absorption coefficients as a function of the transition energy at room temperature. The detailed structure is for structure III in Table II.

first excited level, and so on. We did not observe similar features in the InGaAsN/GaAs QWs[15] with a low confinement, where both the ground and the first excited levels are below E_N. The interesting finding in the GaAsN/AlAs QW with a very deep well can be explained as follows. Due to the fact that the nitrogen level is introduced between the ground level and the first excited level in the conduction band of the GaAsN/AlAs QW, the N repulsion leads to the splitting of the ground level E_1 into an S-like E_{1-} and an S_N-like E_{1+}. Although the first excited level E_2 is much higher than the nitrogen state, it is still affected by the strong repulsion from the N level. The second level splits into a lower S_N-like E_{2-} and a higher S-like E_{2+}, which leads to the anticrossing effect on the dispersion curves, as observed in Fig. 1(b). The dispersion of E_{1-} exhibits a flattening trend (S_N-like) near the nitrogen band as the wave vector increases, while the E_{1+} curve becomes flat (S_N-like) near the nitrogen band as the wave vector approaches zero. In addition, with the variation of the wave vector, the curve of E_{2-} is nearly flat shaped (S_N-like) due to its strong interaction with the N band. From the analysis above, the actual S-like ground level E_1 ought to be E_{1-}, while the S-like first excited level E_2 ought to be E_{2+}. Thereby, the ISBT of $E_1 \rightarrow E_2$ can be attributed to $E_{1-} \rightarrow E_{2+}$. Figure 1(c) further supports this rule. The absorption coefficient is calculated at an electron concentration of 1×10^{18} cm^{-3}. The diagram shows us that the weak low energy transition is built on $E_{1-} \rightarrow E_{2-}$, while the strong high energy transition is built on $E_{1-} \rightarrow E_{2+}$. It can be explained as follows. The S-like E_{2+} contains much less N (at $k=0$) than the S_N-like E_{2-}. Since the N component has no contribution to the transition, the amplitude of the oscillator strength decreases with N concentration. Hence, the absorption coefficients decrease with more N component. A further discussion on the impact of the N component on the ISBTs will be presented later. Our calculated results show that the energy of the ISBT based on the ground level $E_{1-} \rightarrow E_{2+}$ is 730 meV (1.69 μm), which is in good agreement with the responsivity peak of (1.64 μm).[14]

The comparison results of structure II in Table II are shown in Fig. 2. In Fig. 2(a), a new order of E_{1+} and E_{2-} is

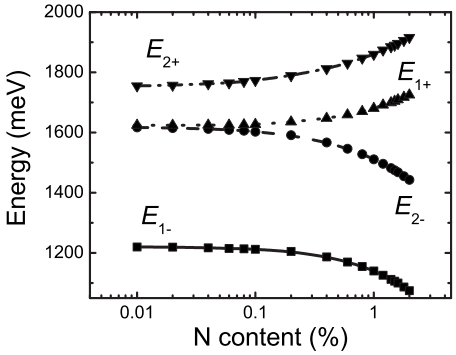

FIG. 4. Energy levels versus N content in an $In_{0.6}Ga_{0.4}As_{1-y}N_y/AlAs$ SQW with a well width of 30 Å and a barrier width of 80 Å. The temperature is 300 K.

TABLE III. Structures of SQWs for comparison with the literature using the ten-band model and the compared results.

Structure No.	Structure	ww (Å)	bw (Å)	T (K)	Expt. (μm)	Calc. (μm)
1	$In_{0.6}Ga_{0.4}As/Al_{0.45}Ga_{0.55}As$ [a]	30	80	300	3.0	2.9
2	$In_{0.6}Ga_{0.4}As/Al_{0.67}Ga_{0.33}As$ [a]	30	80	300	2.6	2.7
3	$In_{0.6}Ga_{0.4}As/AlAs$ [a]	30	80	300	2.2	2.3

[a]Reference 24.

observed. Unlike the results we have observed for structure I, E_{2-} is now conversely above E_{1+}. We will give a more detailed discussion on this point later. The intersubband absorption (ISA) spectra are shown in Fig. 2(b). A high energy peak appears at 740 meV (1.68 μm) with a larger amplitude than the one at low energy side (421 meV). The former transition corresponds to the ISBT from the S-like ground level to the first excited level $E_{1-} \rightarrow E_{2+}$. At the same time, the weak peak results from the ISBT $E_{1-} \rightarrow E_{2-}$, which corresponds to a 2.94 μm ISA. It matches the absorption peak observed in Ref. 23. Since the experimental results did not cover ISA wavelengths below 2.5 μm, we cannot draw a further conclusion on the calculated ISA feature at about 1.68 μm.

Figure 3 shows another comparison with structure III in Table II. The width of the GaAsN well increases from 25 Å for structure II to 55 Å for structure III. As can be observed in Fig. 3(a), all the levels in the conduction band drop with the well width. Even the second excited level E_3 decreases to an energy below the band edge of the AlAs barrier. The calculated ISA spectrum is shown in Fig. 3(b). There are three peaks presented in the figure that correspond to the transitions of $E_{1-} \rightarrow E_{2-}$, $E_{1-} \rightarrow E_{2+}$, and $E_{1-} \rightarrow E_3$ from the low energy to the high energy portions. As the E_{2-} state is N rich, while E_{2+} state contains less N, the intensity of the transition based on E_{2-} is weaker than that of the transition based on E_{2+}. An obvious intersubband transition from E_{1-} to E_3 occurs, which can be explained as follows. Within the multiband scheme, the interaction between the conduction band and the valence band is considered. Such conduction band and valence band mixing enhances the $E_{1-} \rightarrow E_3$ transition. The ISBT of $E_{1-} \rightarrow E_{2+}$ is bound to bound, while $E_{1-} \rightarrow E_3$ is bound to quasicontinuum. It follows that the ISA amplitude of the former transition is larger than that of the latter one, which is in agreement with Fig. 3(b).As a result of the ISA curve, the transition of $E_{1-} \rightarrow E_{2+}$ corresponds to 503 meV (2.46 μm), which is in good agreement with the measured 2.5 μm peak. Because the experimental results lack the wavelength range (between <2 μm and >5 μm) cov-

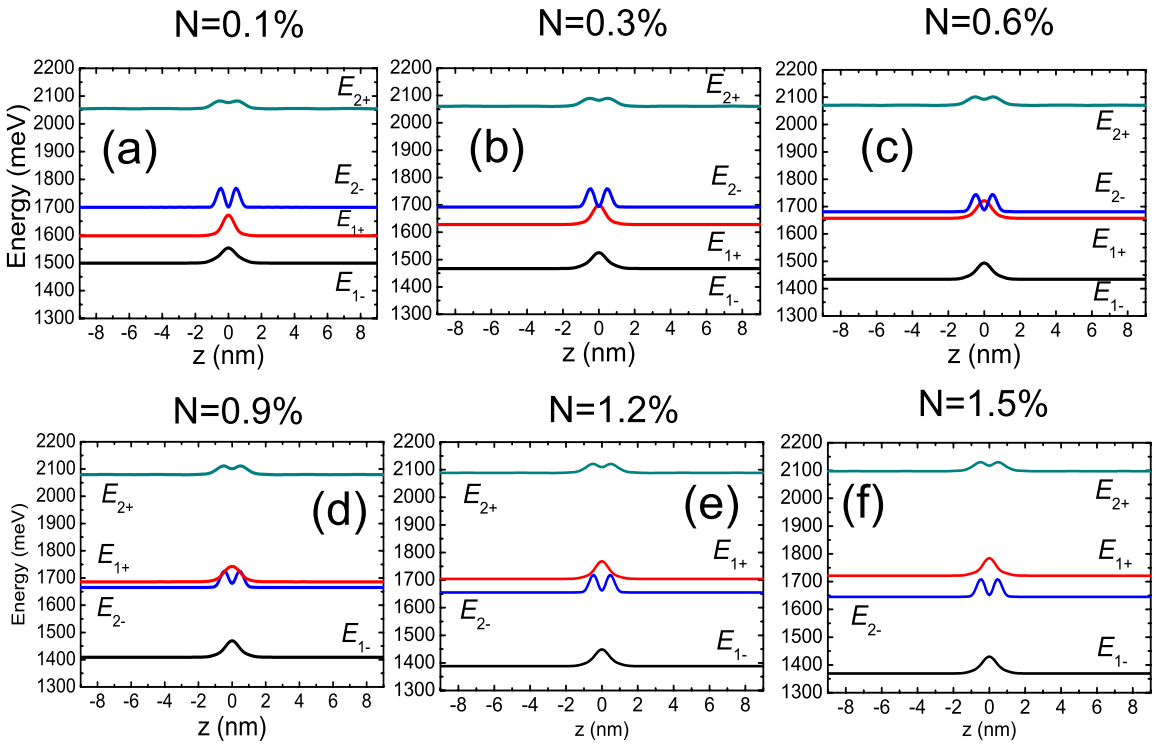

FIG. 5. (Color online) Dependence of the squared wave functions corresponding to the subbands E_{1-}, E_{2-}, E_{1+}, and E_{2+} of an $In_{0.3}Ga_{0.7}As_{1-y}N_y/AlAs/Al_{0.3}Ga_{0.7}As$ DBQW on the N concentration when $k=0$ $(2\pi/L)$. The well width is 20 Å and the temperature is 20 K.

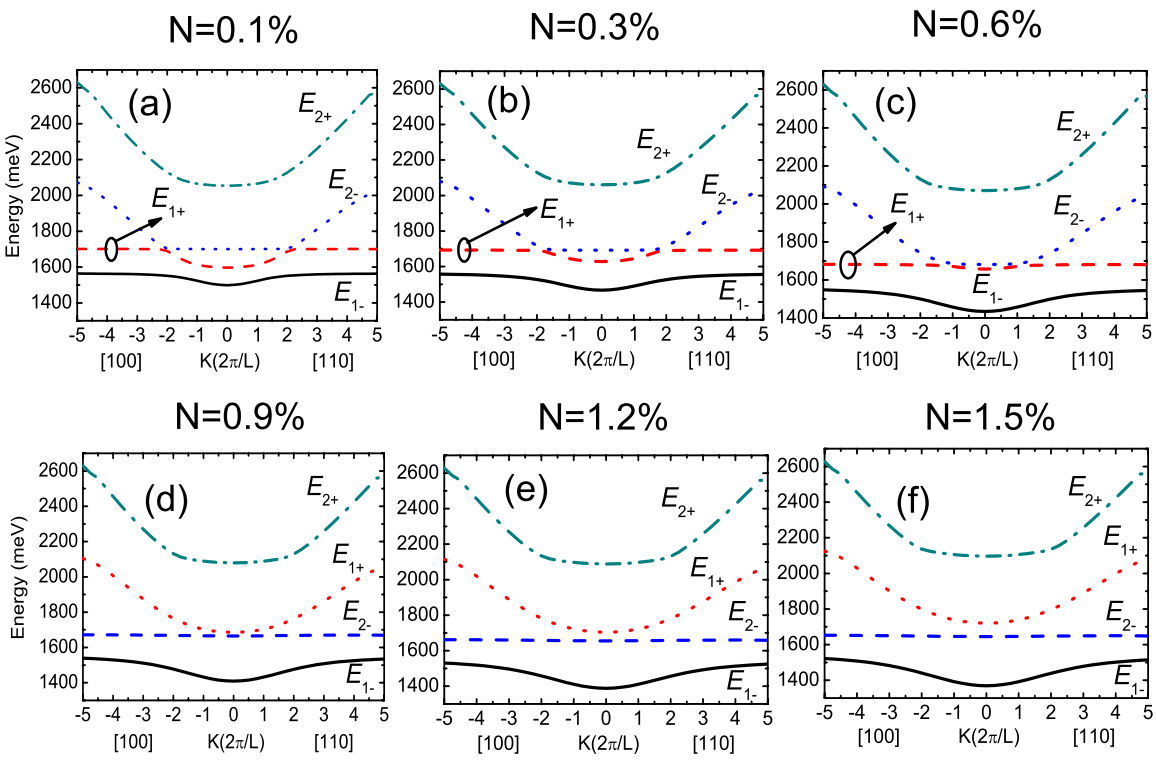

FIG. 6. (Color online) Dependence of energy dispersion curves of the subbands E_{1-}, E_{2-}, E_{1+}, and E_{2+} in the conduction band along the [100] and [110] crystal directions for an $In_{0.3}Ga_{0.7}As_{1-y}N_y/AlAs/Al_{0.3}Ga_{0.7}As$ DBQW on the N concentration. The well width is 20 Å and the temperature is 20 K.

ering the other two peaks, they cannot be compared here.[23]

Additionally, to clarify that our program is valid for the calculation of SQWs, we calculate the conduction-band structure of $In_{0.6}Ga_{0.4}As_{1-y}N_y/Al_zGa_{1-z}As$ SQWs. The N-free samples were investigated experimentally by Chui *et al.*[24] Table III shows that our calculations agree well with their measurements. Subsequently, we use an $In_{0.6}Ga_{0.4}As_{0.99}N_{0.01}/AlAs$ SQW with the same combination as structure III to investigate how the N incorporation affects the energy levels. We calculate the variation of energy levels with the N content in an $In_{0.6}Ga_{0.4}As_{1-y}N_y/AlAs$ QW, as shown in Fig. 4. With an increasing N content, the repulsion strength from the N level increases, which leads to increasing E_{1+} and E_{2+} while decreasing E_{1-} and E_{2-}. This behavior is in agreement with that reported in Ref. 25.

From the comparisons above, we are able to confirm the validity of the ten-band $k\cdot p$ method in calculating InGaAsN DBQWs which have high confinement.

B. Theoretical design of the double-barrier quantum well structures with intersubband absorptions at 1.31 and 1.55 μm

We now present the design procedure for the DBQW structures within which the ISBTs from the ground level to the second level correspond to 1.31–1.55 μm. The band structures and absorptions of the $In_xGa_{1-x}As_{1-y}N_y/AlAs/Al_{0.3}Ga_{0.7}As$ DBQW, with an inner barrier (AlAs) width of 15 Å and an outer barrier (AlGaAs) width of 130 Å, are chosen to be calculated by using the ten-band model at a temperature of 20 K.

For our design, we are first interested to know how the N content impacts the conduction-band structure of the DBQW. The In content is fixed at 30% and the well width is fixed at 20 Å. In this paper, for convenience, we identify subbands according to their properties when $k=0$ $(2\pi/L)$ (we will omit the unit k hereafter).

Figure 5 shows the variation of the squared wave functions of the ground level E_1 and the first excited state E_2 with an increasing N content when the wave vector $k=0$. For simplicity, we will ignore those states in the outer barrier regions. As Fig. 5 indicates, once the N content is introduced in the QWs with large CBO, the states E_1 and E_2 will each split into E_{1-}, E_{1+}, E_{2-}, and E_{2+}. For $N \leq 0.6\%$, the case is somewhat different from that of SQWs. As shown in Figs. 5(a)–5(c), E_{1+} is lower than E_{2-}. As N increases to higher than 0.9%, E_{1+} conversely increases higher than E_{2-}, as shown in Figs. 5(d)–5(f). To help explain this interesting feature, we first plot the energy dispersion curves of the four subbands versus N content in Fig. 6, then plot the squared wave functions for $k=5$ and N=0.1% in Fig. 7, and then show how the concentration of nitrogen atoms impacts the components of N, e, HH, LH, and SO in E_{1-}, E_{1+}, E_{2-}, and E_{2+} states, respectively, in Figs. 8–11. The variation of the energy dispersions with k points follows the rule that for a state that contains more electron components (S-like), the dispersion curve is more parabolic. In contrast, for a state that contains more N components (S_N-like), the curve tends to be flat. Figure 6 indicates that as k becomes higher ($k=5$), the first two levels from the bottom, which tend to be flat, are actually two quantized N levels (in terms of E_{n1} and

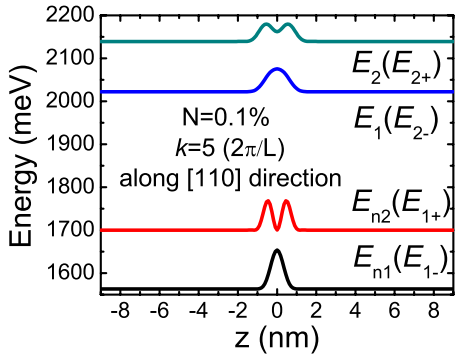

FIG. 7. (Color online) The squared wave functions in the well of an $In_{0.3}Ga_{0.7}As_{0.999}N_{0.001}/AlAs/Al_{0.3}Ga_{0.7}As$ DBQW when $k=5$ $(2\pi/L)$ in the [110] direction. The identification in the parentheses is for $k=0$ $(2\pi/L)$. The well width is 20 Å and the temperature is 20 K.

E_{n2}), while the highest two levels are S-like states (in terms of E_1 and E_2). As can be clearly seen in Fig. 7, the peak of the four wave functions indicates that they are E_{n1}, E_{n2}, E_1, and E_2 counted from the bottom when $k=5$ and N=0.1%. It can also be understood from Figs. 8–11, where N dominates the first two levels and an electron dominates the highest two levels when $k=5$. Due to the fact that the dispersion curves for N states will remain flat as k varies, the positions of the two quantized N states can be found when k is large ($k=5$ is enough). It shows us that E_{1+} and E_{2-} do not converge to a N level as the N content approaches zero, which is caused by the anticrossing effects between the two separate N states and the original E_1 and E_2 states before splitting. That is to say, E_1 interacts with E_{n1} resulting in anticrossed E_{1-} (shift downward) and E_{1+} (shift upward); meanwhile, E_2 interacts with E_{n2} resulting in anticrossed E_{2-} (shift downward) and E_{2+} (shift upward). Initially, the split energy of both E_1 and E_2 is small with a small N content, which causes a higher E_{2-} than E_{1+} and a large separation between them. With more N content added, the split energy of both E_1 and E_2 increases. Thus, the separation between E_{1+} and E_{2-} levels decreases until E_{1+} ultimately increases above E_{2-}. Subsequently, the energy separation between them increases again from then on.

To confirm the analysis above, we further calculated the energy separation of E_{1+} and E_{2-} when the N content is extremely small (about 1×10^{-8}%) and concluded that $E_{1+}=1567$ meV and $E_{2-}=1705$ meV (when $k=0$), while $E_{n1}=1567$ meV and $E_{n2}=1705$ meV (when $k=5$). This clarifies the fact that the difference between E_{1+} and E_{2-} is actually the quantization energy of the N level in the DBQW for an extremely diluted nitrogen content. One should note that the slight drop in N quantized levels with the increasing N content is due to the zero point of E_N, which is taken at the strained valence-band edge in the well. We shall now look more carefully into how the concentration of nitrogen atoms impacts the components of N, e, HH, LH, and SO in E_{1-}, E_{1+}, E_{2-}, and E_{2+} states, respectively. Figures 8–11 show the dependence of the five components in the first four states counted from the bottom of the nitrogen concentration. Considering the dominance of electron at $k=0$, E_{1-} and E_{2+} states

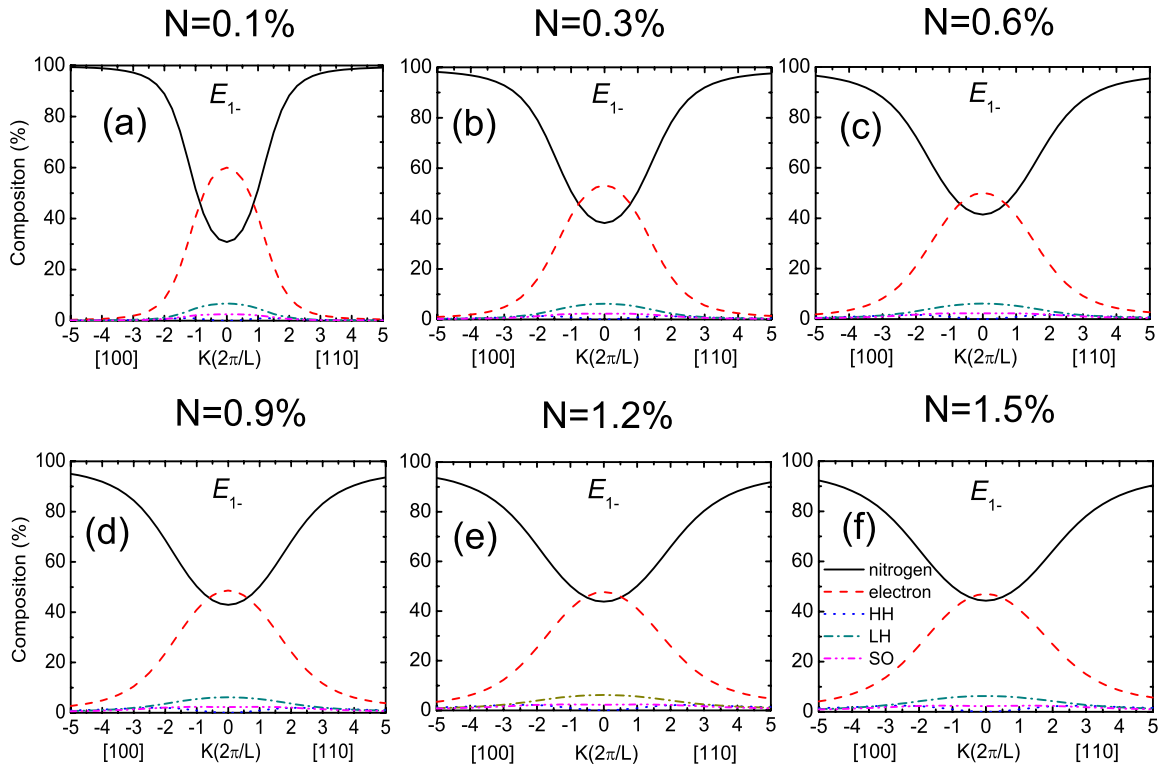

FIG. 8. (Color online) Dependence of the percentage of the components of N, electron, HH, LH, and SO states in the first subband in Fig. 6 on the N concentration. The structure considered is an $In_{0.3}Ga_{0.7}As_{1-y}N_y/AlAs/Al_{0.3}Ga_{0.7}As$ DBQW. The well width is 20 Å and the temperature is 20 K.

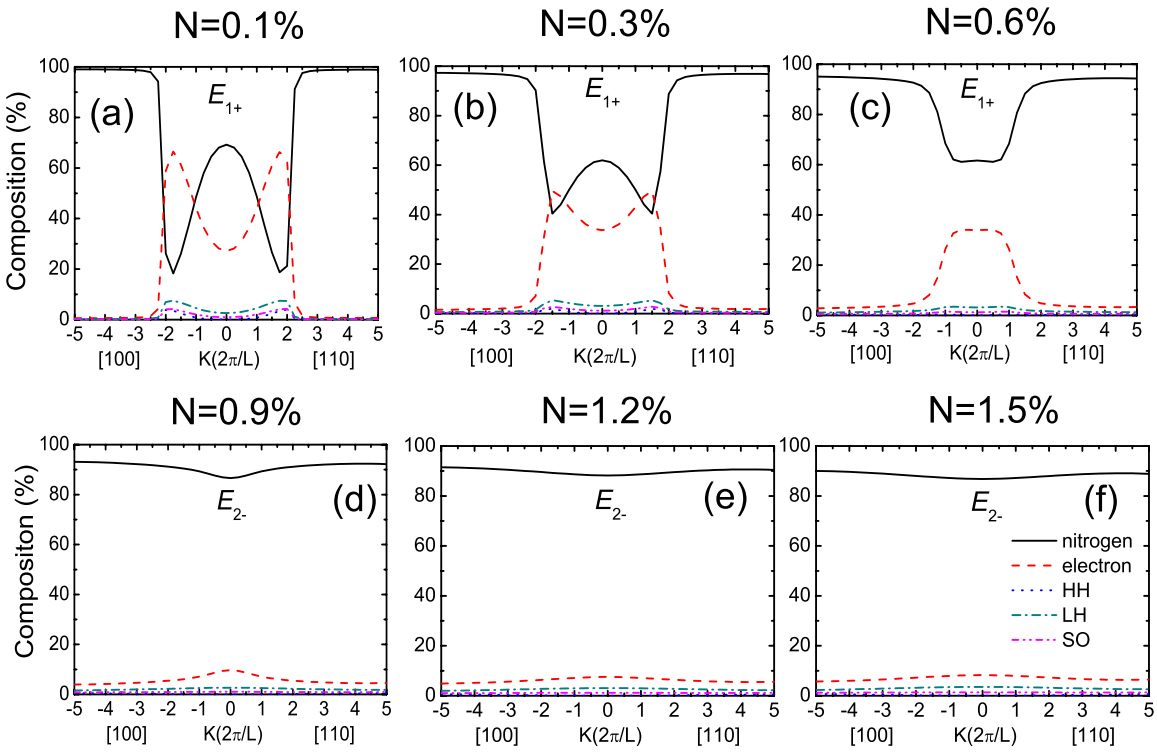

FIG. 9. (Color online) Dependence of the percentage of the components of N, electron, HH, LH, and SO states in the second subband in Fig. 6 on the N concentration. The structure considered is an $In_{0.3}Ga_{0.7}As_{1-y}N_y/AlAs/Al_{0.3}Ga_{0.7}As$ DBQW. The well width is 20 Å and the temperature is 20 K.

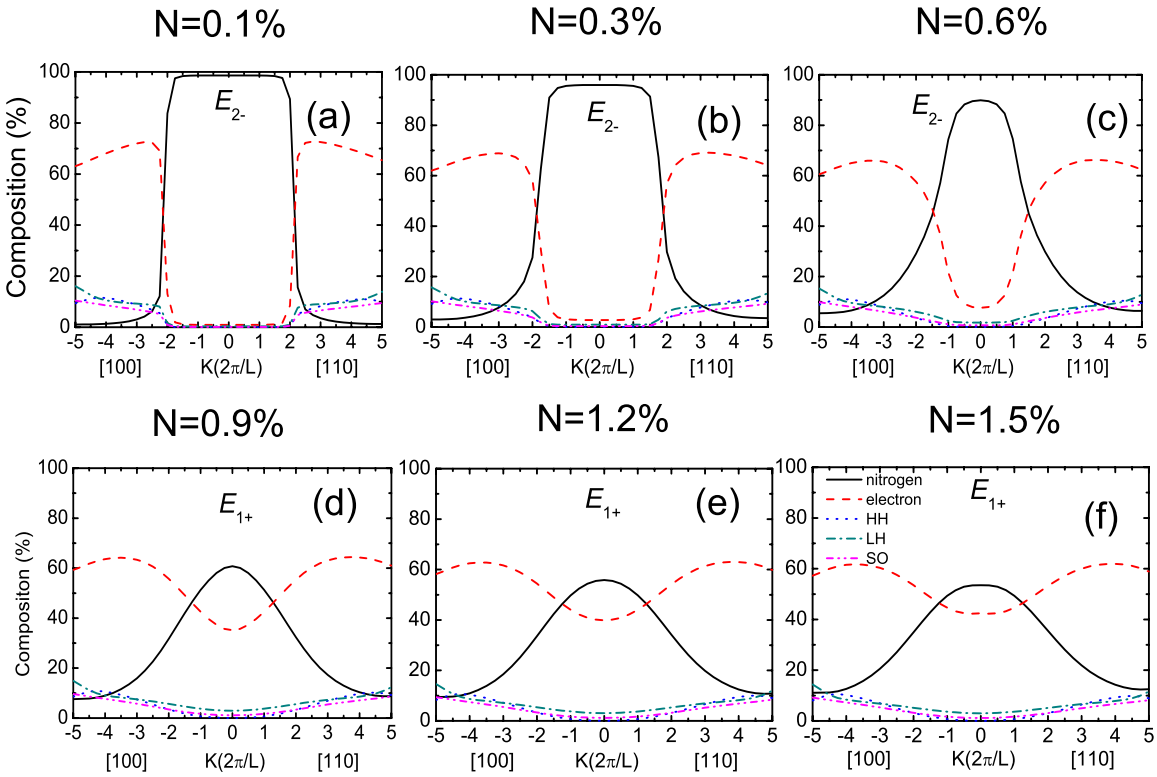

FIG. 10. (Color online) Dependence of the percentage of the components of N, electron, HH, LH, and SO states in the third subband in Fig. 6 on the N concentration. The structure considered is an $In_{0.3}Ga_{0.7}As_{1-y}N_y/AlAs/Al_{0.3}Ga_{0.7}As$ DBQW. The well width is 20 Å and the temperature is 20 K.

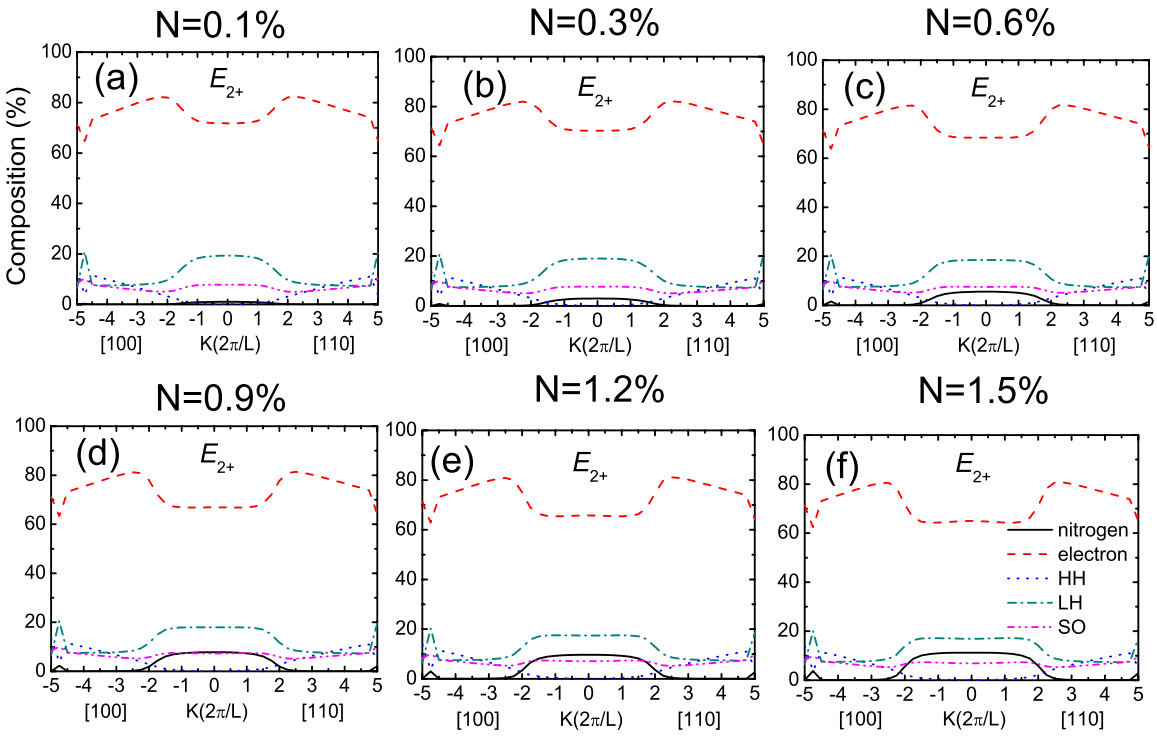

FIG. 11. (Color online) Dependence of the percentage of the components of N, electron, HH, LH, and SO states in the fourth subband in Fig. 6 on the N concentration. The structure considered is an $In_{0.3}Ga_{0.7}As_{1-y}N_y/AlAs/Al_{0.3}Ga_{0.7}As$ DBQW. The well width is 20 Å and the temperature is 20 K.

are *S*-like; on the contrary, the dominant nitrogen component at $k=0$ determines that E_{1+} and E_{2-} are S_N-like. As can also be seen in Figs. 8 and 9, as the nitrogen concentration increases from 0.1% to 1.5%, the N component increases, and the electron component decreases for the first and second levels. However, the contrary holds for the third level, as shown in Fig. 10. This is more evidence confirming that the E_{2-} level drops (contains more N content), while the E_{1+} level rises (contains less N content) so that they will have alternating positions.

Hence, the two discrete N levels sandwiched between the first and the second electron states are the origin of the difference between a DBQW and SQW; that is, the latter contains only one N quantized level between the first and the second electron states.

We now present the subbands and the transition energy in the conduction band of the $In_{0.3}Ga_{0.7}As_{1-y}N_y/AlAs/Al_{0.3}Ga_{0.7}As$ DBQW calculated as a function of the nitrogen composition, as illustrated in Fig. 12(a). As can be observed from Fig. 12(a), as N increases from 0.1% to 1.5%, E_{1-} decreases and E_{2+} increases. This results in an increase in transition energy with N content. As can also be seen in Fig. 12(a), the discrete solid lines identified as B1–B4 are the subbands localized in the AlGaAs barrier. They are nearly unchanged as N increases since the CBOs of AlGaAs/AlAs are constant. The ISA spectra as a function of the N content calculated by our model are shown in Fig. 12(b) with a doping concentration of 1×10^{18} cm^{-3}. Contrary to Figs. 1–3, the absorption peak of the $E_{1-}\rightarrow E_{2-}$ transition for the present case can be ignored. We attribute the decrease of this peak to the narrow-well-width effect. The E_{2-} level is pushed upward with a reduction in the well width so that the oscillator strength decreases. The energy of the ISBT increases from 521 to 727 meV with N content which shows an obvious blueshift.

We are now in a position to study how the InGaAsN well width impacts the energy levels and the transition energy in the DBQW structure. The results are shown in Fig. 13(a). As can be seen, all the four levels E_{1-} to E_{2+} reduce with the well width from 20 to 50 Å. The highest level E_{2+} drops from above the fourth level in the AlGaAs barrier to a state lower than the first level in the AlGaAs barrier. As for the case considered here, the In content and the N content are equal to 30% and 1.5% in the well, respectively. E_{1+} is always above E_{2-} as the well width increases. Now, we discuss the ISA spectra as a function of the well width. The results are shown in Fig. 13(b) with a doping concentration of 1×10^{18} cm^{-3}. When the well width increases, the amplitude of the peaks corresponding to the transition of $E_{1-}\rightarrow E_{2+}$ (high energy one) slightly decreases. On the other hand, the lower energy peaks based on the E_{1-} to E_{2-} transition become stronger with the well width. This can be explained as follows. Due to the fact that E_{2-} tends to be far away from the N levels while E_{2+} tends toward the N levels with a wider well, the oscillation strength of the ISBT $E_{1-}\rightarrow E_{2+}$ decreases while that of the ISBT $E_{1-}\rightarrow E_{2-}$ increases. Consequently, the ISBT energy redshifts from 727 to 482 meV as the well width increases.

The subbands and the transition energy in the conduction band of the InGaAsN DBQW calculated as a function of the indium composition are illustrated in Fig. 14. When In increases from 0% to 30%, all four levels E_{1-} to E_{2+} drop.

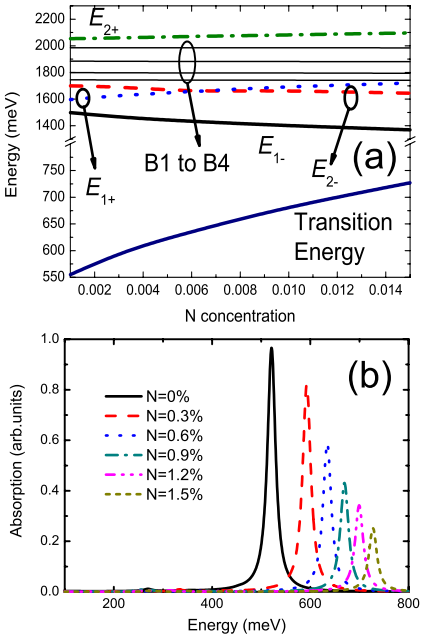

FIG. 12. (Color online) (a) Dependence of the subbands E_{1-}, E_{2-}, E_{1+}, and E_{2+} and the energy separation between the ground and the first excited levels ($E_{1-} \rightarrow E_{2+}$) in the conduction band for an $In_{0.3}Ga_{0.7}As_{1-y}N_y/AlAs/Al_{0.3}Ga_{0.7}As$ DBQW on the N concentration. The solid lines are the subbands localized in the AlGaAs barrier ($E_1 \rightarrow E_4$ from bottom to top). (b) Dependence of the absorption coefficients on the N concentration. The well width is 20 Å and the temperature is 20 K.

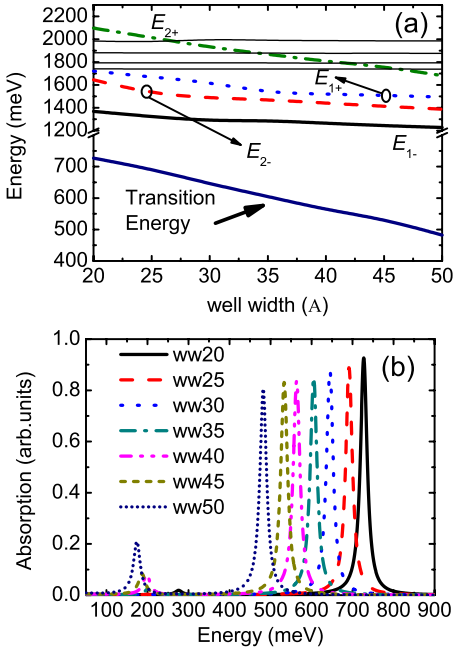

FIG. 13. (Color online) (a) Dependence of the subbands E_{1-}, E_{2-}, E_{1+}, and E_{2+} and the transition energy $E_{1-} \rightarrow E_{2+}$ in the conduction band of an $In_{0.3}Ga_{0.7}As_{0.985}N_{0.015}/AlAs/Al_{0.3}Ga_{0.7}As$ DBQW on the InGaAsN well width. The solid lines are the subbands localized in the AlGaAs barrier ($E_1 \rightarrow E_4$ from bottom to top). (b) Dependence of the absorption coefficients for the DBQW on the InGaAsN well width. All the calculations are at 20 K.

Figure 14(b) shows the ISA spectra as a function of the In content. The doping concentration is 1×10^{18} cm^{-3}. When In increases, the amplitude of the peaks corresponding to the transition of $E_{1-} \rightarrow E_{2+}$ (high energy one) increases because the N component contained in E_{1-} decreases. When In $<10\%$ and $>15\%$, the increase in the amplitude is slight. However, it increases greatly when In increases from 10% to 15%. This is due to the fact that the transition type changes from bound→bound to bound→continuum with respect to the AlAs barrier edge. There are other low energy peaks based on the E_{1-} to E_{2-} transition which are negligible. They are the results of the narrow-well-width (20 Å) effect mentioned above. As a result, the ISBT energy decreases from 1052 to 727 meV with increasing In concentration.

Finally, our design procedure using the ten-band model, as shown in Figs. 12–14, proposes two structures. One is the $In_{0.17}Ga_{0.83}As_{0.985}N_{0.015}/AlAs/Al_{0.3}Ga_{0.7}As$ DBQW with a well width of 20 Å, an AlAs barrier width of 15 Å, and an AlGaAs barrier width of 130 Å. At 20 K, it can achieve an ISA peak at about 1.31 μm (947 meV). The other one is the In composition of 25% (the other parameters are the same as above), which may achieve an ISA peak at about 1.55 μm (800 meV).

IV. SUMMARY AND CONCLUSIONS

In conclusion, a study of the $In_xGa_{1-x}As_{1-y}N_y/AlAs/Al_{0.3}Ga_{0.7}As$ DBQW structures has been reported within the ten-band $k \cdot p$ scheme. This material system is very promising

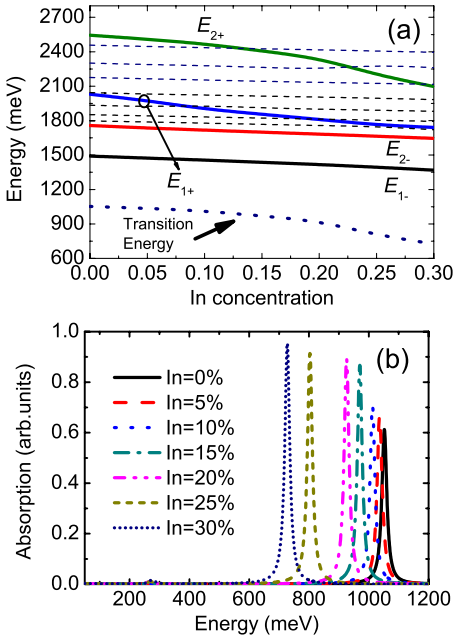

FIG. 14. (Color online) (a) Dependence of the subbands E_{1-}, E_{2-}, E_{1+}, and E_{2+} and the transition energy $E_{1-} \rightarrow E_{2+}$ in the conduction band of an $In_xGa_{1-x}As_{0.985}N_{0.015}/AlAs/Al_{0.3}Ga_{0.7}As$ DBQW on the In concentration of the InGaAsN alloy. The discrete dashed lines are the subbands localized in the AlGaAs barrier ($E_1 \rightarrow E_7$ from bottom to top). (b) Dependence of the absorption coefficients for the DBQW on the In concentration. All the calculations are for ww=20 Å at 20 K.

for the production of intersubband absorptions in the 1.31–1.55 μm optical communication wavelength region, thanks to its large CBO. We find that for the QWs with an N level sandwiched between the ground and the first excited levels, the first two subbands are split. This effect is very useful in shortening the ISA wavelengths. We conclude that the energy of the ISBT within the QW increases with the N concentration; by contrast, it decreases with the well width and the In concentration, respectively. By carefully tailoring the compositions, the structures have been obtained to achieve ISA wavelengths of 1.31 and 1.55 μm.

ACKNOWLEDGMENTS

One of the authors (W.J.F.) would like to acknowledge the support for this work from A*star (Grant No. 0421010077). The authors would like to thank X. W. Zhang, B. S. Ma, and S. T. Ng for valuable discussions.

*ewjfan@ntu.edu.sg

[1] B. F. Levine, J. Appl. Phys. **74**, R1 (1993).
[2] M. P. Semtsiv, M. Ziegler, W. T. Masselink, N. Georgiev, T. Dekorsy, and M. Helm, J. Appl. Phys. **97**, 113538 (2005).
[3] C. P. Garcia, A. D. Nardis, V. Pellegrini, J. M. Jancu, F. Beltram, B. H. Mueller, L. Sorba, and A. Franciosi, Appl. Phys. Lett. **77**, 3767 (2000).
[4] H. C. Liu, P. H. Wilson, M. Lamm, A. G. Steele, Z. R. Wasilewski, J. M. Li, M. Buchanan, and J. G. Simmons, Appl. Phys. Lett. **64**, 475 (1994).
[5] H. Schneider, F. Fuchs, B. Dischler, J. D. Ralston, and P. Koidl, Appl. Phys. Lett. **58**, 2234 (1991).
[6] J. H. Lee, J. C. Chiang, S. S. Li, and P. J. Kannam, Appl. Phys. Lett. **74**, 765 (1999).
[7] K. T. Lai, M. Missous, R. Gupta, and S. K. Haywood, J. Appl. Phys. **93**, 6065 (2003).
[8] C. W. Cheah, G. Karunasiri, L. S. Tan, and L. F. Zhou, Appl. Phys. Lett. **80**, 145 (2002).
[9] M. Z. Tidrow, K. K. Choi, A. J. Deanni, W. H. Chang, and S. P. Suensson, Appl. Phys. Lett. **67**, 1800 (1995).
[10] Q. J. Chen, K. K. Choi, W. H. Chang, and D. C. Tsui, Appl. Phys. Lett. **72**, 7 (1998).
[11] K. K. Choi, S. V. Bandara, S. D. Gunapala, W. K. Liu, and J. M. Fastenav, J. Appl. Phys. **91**, 551 (2002).
[12] M. Z. Tidrow, J. C. Chiang, S. S. Li, and K. Bacher, Appl. Phys. Lett. **70**, 859 (1997).
[13] J. J. Shi and E. M. Goldys, IEEE Trans. Electron Devices **46**, 83 (1999).
[14] E. Luna, M. Hopkinson, J. M. Ulloa, A. Guzman, and E. Munoz, Appl. Phys. Lett. **83**, 3111 (2003).
[15] S. T. Ng, W. J. Fan, Y. X. Dang, and S. F. Yoon, Phys. Rev. B **72**, 115341 (2005).
[16] M. Galluppi, L. Geelhaar, and H. Riechert, Appl. Phys. Lett. **86**, 131925 (2005).
[17] S. T. Ng, W. J. Fan, S. F. Yoon, S. Z. Wang, Y. Qu, C. Y. Liu, S. G. Ma, and S. Yuan, J. Appl. Phys. **96**, 4663 (2004).
[18] S. T. Ng, W. J. Fan, Y. X. Dang, and S. F. Yoon, Jpn. J. Appl. Phys., Part 2 **44**, L658 (2005).
[19] Y. X. Dang, W. J. Fan, S. T. Ng, S. Wicaksono, S. F. Yoon, and D. H. Zhang, J. Appl. Phys. **98**, 026102 (2005).
[20] I. Vurgaftman, J. R. Meyer, and L. R. Ram-Mohan, J. Appl. Phys. **89**, 5815 (2001).
[21] I. Vurgaftman and J. R. Meyer, J. Appl. Phys. **94**, 3675 (2003).
[22] D. J. Arent, Phys. Rev. B **41**, 9843 (1990).
[23] A. Guzmán, E. Luna, J. Miguel-Sánchez, E. Calleja, and E. Munoz, Infrared Phys. Technol. **44**, 377 (2003).
[24] H. C. Chui, E. L. Martinet, M. M. Fejer, and J. S. Harris, Jr., Appl. Phys. Lett. **64**, 736 (1994).
[25] Jean-Yves Duboz, Phys. Rev. B **75**, 045327 (2007).